The current issue and full text archive of this journal is available at
www.emeraldinsight.com/0961-5539.htm

A numerical model for the thermocapillary flow and heat transfer in a thin liquid film on a microstructured wall

Received 1 January 2006
Accepted 9 July 2006

A. Alexeev
Department of Chemical Engineering, University of Pittsburgh, Pittsburgh, Pennsylvania, USA, and
T. Gambaryan-Roisman and P. Stephan
Darmstadt University of Technology, Darmstadt, Germany

Abstract

Purpose – This paper aims to study thermocapillarity-induced flow of thin liquid films covering heated horizontal walls with 2D topography.

Design/methodology/approach – A numerical model based on the 2D solution of heat and fluid flow within the liquid film, the gas above the film and the structured wall is developed. The full Navier-Stokes equations are solved and coupled with the energy equation by a finite difference algorithm. The movable gas-liquid interface is tracked by means of the volume-of-fluid method. The model is validated by comparison with theoretical and experimental data showing a good agreement.

Findings – It is demonstrated that convective motion within a film on a structured wall exists at any nonzero Marangoni number. The motion is caused by surface tension gradients induced by temperature differences at the gas-liquid interface due to the spatial structure of the heated wall. These simulations predict that the maximal flow velocity is practically independent from the film thickness, and increases with increasing temperature difference between the wall and the surrounding gas. It is found that an abrupt change in wall temperature causes rupture of the liquid film. The thermocapillary convection notably enhances heat transfer in liquid films on heated structured walls.

Research limitations/implications – Our solutions are restricted to the case of periodic wall structure, and the flow is enforced to be periodic with a period equal to that of the wall.

Practical implications – The reported results are useful for design of the heat transfer equipment.

Originality/value – New effects in thermocapillary convection are presented and studied using a developed numerical model.

Keywords Volume measurement, Fluid dynamics, Numerical control, Convection, Heat transfer

Paper type Research paper

Nomenclature

A	= wall structure amplitude	c_p	= specific heat capacity
Bi	= Biot number	d	= wall structure period
C	= color function	$\mathbf{F}$	= body forces
$\tilde{C}$	= averaged color function	$\mathbf{F}_s$	= body force due to surface tension

The authors would like to acknowledge the generous support of the German Science Foundation, DFG, through the Emmy Noether Program. A. Alexeev is grateful to Virgil Stoica for his assistance in the conduction of the experiments.

International Journal of Numerical Methods for Heat & Fluid Flow
Vol. 17 No. 3, 2007
pp. 247-262

0961-5539
DOI 10.1108/09615530710730139

h_g = gas layer thickness
h_w = wall structure height
Δh = average thickness of liquid film
Δh^* = minimal thickness of liquid film
k = interface curvature
M = Marangoni number
M_{cr} = critical Marangoni number
$\mathbf{n}$ = unit normal to interface
Nu = Nusselt number
p = pressure
S = interface "height" function
t = time
T = temperature
ΔT = temperature drop
$\mathbf{u}$ = velocity
u_{max} = maximal liquid velocity at interface

Greek symbols
α = thermal diffusivity
δ_s = Dirac distribution function at interface
λ = thermal conductivity
μ = dynamic viscosity
ρ = density
σ = surface tension
σ_T = temperature coefficient of surface tension
τ = shear stress tensor
φ = wall structure angle

Superscripts
n = iteration level

Subscripts
0, g = gas
1 = liquid
i, j = computational cell index
w = wall

Introduction

Surface tension is crucial in the dynamics of thin liquid films on substrates of different topography, which are frequently encountered in many engineering applications, including the thermal management of electronic devices, food processing, chemical engineering, MEMS.

Normally, the surface tension of a liquid is a decreasing function of temperature. If the temperature varies at the gas-liquid interface, surface tension gradients cause thermocapillary (Marangoni) flow (Colinet *et al.*, 2001). If a thin liquid film is heated on a planar substrate of a uniform temperature, a conducting solution exists, which implies that the film is motionless and the free surface of the liquid is isothermal. This solution is stable for sufficiently small temperature gradients across the liquid layer. If the temperature gradient exceeds a critical value, the conducting solution loses stability and convective patterns are developed (Pearson, 1958). If the substrate has a structure on its surface, the convection prevails for any temperature difference (Alexeev *et al.*, 2005). It occurs due to the temperature inhomogeneity, which is imposed on the interface by the spatial structure of the substrate.

We develop a numerical model to describe the motion of a thin liquid film on a heated structured wall. We deploy a finite difference algorithm to integrate the Navier-Stokes and energy equations. To cope with the movable gas-liquid interface, we apply the volume-of-fluid (VOF) method (Scardovelli and Zaleski, 1999). The calculations are performed simultaneously through the whole computational domain containing the gas and liquid regions, while the surface force at the interface is included into the momentum balance equations via a volumetric force (Kothe and Mjolsness, 1992). The energy equation is solved within the solid wall as well.

There are only few previous studies where the Marangoni flows in a cavity are considered in the framework of the VOF. Sasmal and Hochstein (1994) calculated the Marangoni convection induced by a temperature difference between the sidewalls of a rectangular cavity. They studied heat transfer within the cavity and the effect of the contact angle on the flow patterns. More recently, Wang (2002) applied a VOF model to

investigate the Marangoni convection in trapezoidal cavities. In these works, the temperature gradient was caused by a temperature difference between the sidewalls. Thus, the heat flux was mostly directed along the gas-liquid interface, in that way it was justified to neglect its component normal to the interface by considering the adiabatic condition at the free surface. In contrast, in a flow on a heated structured wall, the heat flux is practically perpendicular to the gas-liquid interface resulting in a strong temperature gradient in that direction. In this case, the thermocapillary force is induced by a relatively small variation of the liquid temperature along the interface. Hence, a very accurate calculation of the temperature is required to avoid unphysical flow currents due to inaccuracy in the temperature gradient evaluation.

In present work, we study thermocapillary motion within a thin film of a low volatility liquid on a heated highly thermal conductive wall with 2D microscale topography. We consider a situation where the liquid layer covers a horizontal wall, and its thickness is comparable with the amplitude of the wall microstructure. We neglect the effect of gravity. Our solutions are restricted to the case of periodic wall structure, and the flow is enforced to be periodic with a period equal to that of the wall.

Numerical model

Governing equations

The incompressible flow is governed by the continuity equation:

$$\nabla \cdot \mathbf{u} = 0, \tag{1}$$

and the Navier-Stokes equations:

$$\rho\left(\frac{\partial \mathbf{u}}{\partial t} + \mathbf{u} \cdot \nabla \mathbf{u}\right) = -\nabla p + \nabla \cdot \boldsymbol{\tau} + \mathbf{F}, \tag{2}$$

where $\mathbf{u}$ is the velocity, ρ the density, p the pressure, $\mathbf{F}$ the body forces, and t time. Moreover, $\boldsymbol{\tau}$ is the shear stress tensor given by:

$$\boldsymbol{\tau}_{ij} = \frac{\mu}{2}\left(\frac{\partial u_j}{\partial x_i} + \frac{\partial u_i}{\partial x_j}\right), \tag{3}$$

where μ is the dynamic viscosity.

The equations are coupled with the energy equation given by:

$$\rho c_{\mathrm{p}}\left(\frac{\partial T}{\partial t} + \mathbf{u} \cdot \nabla T\right) = \nabla \cdot \lambda \nabla T, \tag{4}$$

where T is the temperature, c_{p} the specific heat capacity, and λ the thermal conductivity.

To track the moving gas-liquid interface, we utilize the VOF technique (Scardovelli and Zaleski, 1999). A color function C is introduced, which equals to 1 within the liquid and to 0 within the gas. The color function is governed by a transport equation:

$$\frac{\partial C}{\partial t} + \mathbf{u} \cdot \nabla C = 0. \tag{5}$$

We are looking for the solutions, which are characterized by a period equal to that of the wall structure, d (Figure 1). Thus, we impose a symmetry boundary condition at

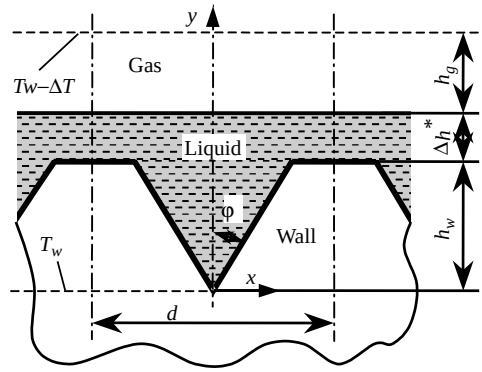

Figure 1.
Outline of the structured wall from the experiments

$x = 0$ and $x = d/2$. We also impose $T = T_w$ at $y = 0$ and $T = T_w - \Delta T$ at $y = h_w + \Delta h^* + h_g$. Moreover, a free flow condition for the velocity ($\partial \mathbf{u}/\partial y = 0$) is applied at $y = h_w + \Delta h^* + h_g$.

Numerical method

The hydrodynamic equations (1)-(3) are solved with a finite difference algorithm on a rectangular staggered grid using the projection method (Ferziger and Peric, 2002). The projection method consists of three steps. First, the prediction velocity field $\mathbf{u}^*$ due to the advective and diffusive terms in equation (2) is to calculate semi-implicitly:

$$\frac{\Delta \mathbf{u}}{\Delta t} + \mathbf{u}^n \cdot \nabla \Delta \mathbf{u} - \frac{1}{\rho^n} \nabla \cdot \Delta \boldsymbol{\tau} = -\mathbf{u}^n \cdot \nabla \mathbf{u}^n + \frac{1}{\rho^n} \nabla \cdot \boldsymbol{\tau}^n + \frac{1}{\rho^n} \mathbf{F}^n, \tag{6}$$

where $\Delta \mathbf{u} = \mathbf{u}^* - \mathbf{u}^n$ and $\Delta \boldsymbol{\tau} = \boldsymbol{\tau}^* - \boldsymbol{\tau}^n$. Then, the Poisson equitation, which is obtained using equation (1), is solved to calculate the pressure field:

$$\nabla \cdot \left(\frac{1}{\rho^n} \nabla p^{n+1} \right) = \frac{\nabla \cdot \mathbf{u}^*}{\Delta t}. \tag{7}$$

Finally, the velocity field is corrected to the time level $n + 1$:

$$\mathbf{u}^{n+1} = \mathbf{u}^* + \frac{\Delta t}{\rho^n} \nabla \cdot \mathbf{u}^*. \tag{8}$$

Using the velocity field $\mathbf{u}^{n+1}$, the color function is advected by solving:

$$\frac{\Delta C}{\Delta t} + \mathbf{u}^{n+1} \cdot \nabla \Delta C = -\mathbf{u}^{n+1} \cdot \nabla C^n, \tag{9}$$

where $\Delta C = C^{n+1} - C^n$. The final stage of the numerical solution involves calculation of the temperature field:

$$\frac{\Delta T}{\Delta t} + \mathbf{u}^{n+1} \cdot \nabla \Delta T - \frac{1}{(c_p \rho)^{n+1}} \nabla \cdot \lambda^{n+1} \nabla \Delta T$$

$$= -\mathbf{u}^{n+1} \cdot \nabla T^n + \frac{1}{(c_p \rho)^{n+1}} \nabla \cdot \lambda^{n+1} \nabla T^n. \quad (10)$$

Here, $\Delta T = T^{n+1} - T^n$.

The advection terms in the r.h.s. of equations (6), (9) and (10) are solved with the third order essentially non-oscillatory (ENO) scheme (Shu and Osher, 1988), while the terms in the advection terms in the l.h.s. of these equations as well as the viscous and conductivity terms are approximated with the second order finite differences. The ENO scheme is used since it provides good tracking of the discontinuity-like interfaces. To treat implicit parts of equations (6), (9) and (10), we utilize the approximate factorization approach and solve the equations separately along the x- and y-directions. The overall accuracy of our method is of the second order in space.

The multigrid technique (Wesseling, 1991) is applied to solve the Poisson equitation for pressure (equation (7)). We use v-cycle and the number of multigrid levels K is given by $3 \times 2^K = \min(N_x, N_y)$, where N_x and N_y are the grid size in the x- and y-directions, respectively. The use of the multigrid technique reduces the overall computational time by an order of magnitude as compared to the standard iterative methods.

To impose the non-slip velocity condition at the liquid-solid boundary, we utilize the immersed boundary approach. We set the x and y velocity components within the solid domain at the nodes right next to the liquid-solid interface such that the linearly interpolated velocity at the interface equals to zero. We also set at these nodes a zero gradient for pressure, while solving equation (7).

Following the VOF approach, we calculate the values of density and viscosity used in equations (6)-(10) as:

$$\rho = (1 - \tilde{C})\rho_0 + \tilde{C}\rho_1, \quad \mu = (1 - \tilde{C})\mu_0 + \tilde{C}\mu_1 \quad (11)$$

Hereafter, the index 1 stands for the liquid, while the index 0 denotes the gas properties. Moreover, $\tilde{C}$ is the averaged color function (Alexeev *et al.*, 2005).

Accurate calculation of the temperature distribution along the gas-liquid interface is critical for a correct modeling of thermocapillary driven flows. When the heat flux is directed across the interface, the difficulty arises due to the discontinuity of properties of the fluids across the interface. In this case, the cell average values cannot provide a satisfactory description for the fluid properties at the interface. In particular, our simulations show that the use of an averaging, either algebraic or geometric, for the calculation of λ causes spurious currents in the fluids.

Mehdi-Nejad *et al.* (2005) have recently developed an approach for a more accurate calculation of the convection terms in the energy equation. They successfully applied this approach to study heat transfer in molten tin drops during their fall. In the case of thermocapillary driven flows on heated walls, however, the heat flux across the interface is typically dominated by the diffusive rather than convective terms. We, therefore, propose a simple approach to calculate the temperature flux across the interface. Consider an interface that is located at the cell (i, j) such that the upper and bottom boundaries of the cell are along the interface (Figure 2). To resolve the diffusive

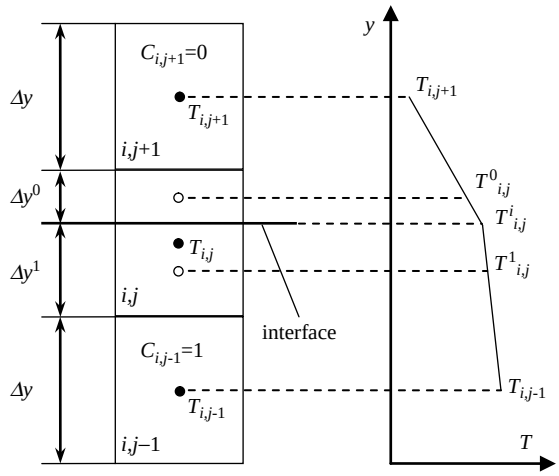

Figure 2.
Schematic diagram of computational cells near the interface and an approximation of the temperature distribution across the interface

terms in equation (10), we approximate the heat fluxes across the bottom and upper boundaries of (i,j) as:

$$f_y^- = 2\lambda_1 \frac{T^1_{i,j} - T_{i,j-1}}{\Delta y + \Delta y^1} \text{ and } f_y^+ = 2\lambda_0 \frac{T_{i,j+1} - T^0_{i,j}}{\Delta y + \Delta y^0}, \tag{12}$$

respectively. Here, $\Delta y^1 = C_{i,j}\Delta y$, $\Delta y^0 = (1 - C_{i,j})\Delta y$ and Δy is the computational grid step. The temperatures $T^0_{i,j}$ and $T^1_{i,j}$ are calculated using two conditions: continuity of the temperature at the interface:

$$T^i_{i,j} = T_{i,j+1} + \left(T^0_{i,j} - T_{i,j+1}\right) \frac{\Delta y + 2\Delta y^0}{\Delta y + \Delta y^0}, \tag{13a}$$

$$T^i_{i,j} = T_{i,j-1} + \left(T^1_{i,j} - T_{i,j-1}\right) \frac{\Delta y + 2\Delta y^1}{\Delta y + \Delta y^1}. \tag{13b}$$

and energy conservation within the cell (i,j):

$$\rho c_p T_{i,j} = (\rho c_p)_0 T^0_{i,j}(1 - C_{i,j}) + (\rho c_p)_1 T^1_{i,j} C_{i,j}, \tag{14}$$

where:

$$\rho c_p = (1 - C_{i,j})(\rho c_p)_0 + C_{i,j}(\rho c_p)_1. \tag{15}$$

Combining equations (13)-(15), $T^0_{i,j}$ and $T^1_{i,j}$ can be readily calculated. These temperatures are also used to evaluate the temperature gradients within the liquid near the gas-liquid interface needed to calculate the thermocapillary force acting at the interface.

To estimate the heat flux component, which is directed along the interface at the cell (i,j), an algebraic averaging for λ is used (equation (10)). At the liquid-solid interface,

where we do not need an accurate value of the temperature gradients, the geometric averaging is used to assess the vertical heat flux, while the algebraic averaging is applied in the horizontal direction.

To illustrate the method for the temperature calculation, we solve equation (10) for a test problem in which the interface between two motionless fluids ($\mathbf{u} = 0$) is slightly inclined and the heat flux is due to a temperature difference between the upper and lower walls (Figure 3(a)). In Figure 3(b) and (c), we present the x and y components of the temperature gradient along the interface, respectively. We are interested in the temperature gradient since the thermocapillary force is directly proportional to its magnitude. To compare with our approach, we also include the results for the temperature gradients calculated with the algebraic and geometric averaging of the thermal conductivity within the numerical cells at the interface.

One can expect for the considered problem (Figure 3(a)) that the interface temperature changes monotonically, meaning that the magnitude of the temperature gradient may not oscillate along the interface. Nevertheless, both the algebraic and geometric averaging results in strong oscillations of the temperature gradient with a period which is correlated with the numerical grid spacing. These oscillations eventually cause spurious currents along the interface induced by the unphysical variations in the thermocapillary force. In contrast, our approach gives a much better approximation of the gradients along the interface. Although there is still some noise in $\partial T/\partial x$ due to the discretization, it can be reduced by applying an appropriate smoothing. Our simulations, however, show that this noise practically does not affect the results.

To include the effect of surface tension into the momentum equations, we adopt the continuum surface force approach (Kothe and Mjolsness, 1992). The body force due to surface tension is given by:

$$\mathbf{F}_{\mathrm{s}} = \frac{2\rho\delta_{\mathrm{s}}}{(\rho_0 + \rho_1)}[\sigma k\mathbf{n} + (1 - \mathbf{n}\otimes\mathbf{n})\nabla\sigma], \tag{16}$$

where σ is the surface tension, $\delta_{\mathrm{s}} = |\nabla\tilde{C}|$ is the Dirac distribution function at the interface, k is the curvature of the interface, and $\mathbf{n}$ is the unit normal to the interface. Moreover, $\nabla\sigma = \sigma_{\mathrm{T}}\nabla T$, where σ_{T} is the temperature coefficient of surface tension. To obtain ∇T at the gas-liquid interface, we calculate the temperature gradients at the cells near the interface, which are filled with the liquid, and then extrapolate the gradients to the interface. To assess the unit normal $\mathbf{n}$ and the curvature of the interface k, we utilize a reconstruction algorithm (Sussman, 2003), which is based on reconstructing the "height" function S directly from the color function C.

Although the ENO scheme, which is used to calculate C provides good tracking of the interface, it causes some numerical "foam" around the interface, which can be accumulated during long time calculations. We, therefore, restore C near the interface in such a way that the "height" functions S and the normal $\mathbf{n}$ remain unchanged, while the "foam" is eliminated. In fact, this procedure breaks the global mass conservation. Our simulations show, however, that the change of the mass is rather small and usually does not exceed 10^{-3} of its initial value even for long calculations.

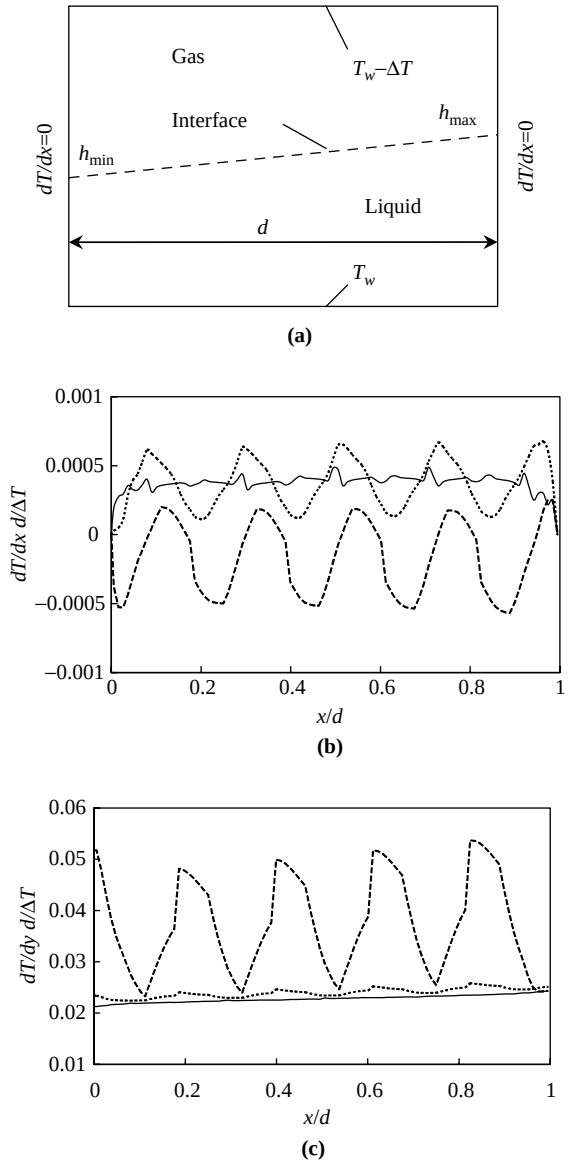

Notes: The domains have thermal properties of a gas (air) and a liquid (water). Grid size is 96×96; domain size is $h = 0.5\ (h_{min} + h_{max}) = 1$ mm, $\Delta h = h_{max} - h_{min} = 0.1$ mm ($\sim 5\Delta y$), $d = 5$mm; $\Delta T = -10$K: (a) schematic of the test problem; (b) and (c), respectively, represent the horizontal and vertical components of the temperature gradient along the interface calculated for different approximations for λ. The solid lines show the approximation of equations (12)-(15), the dotted and dashed lines are for the algebraic and geometric averaging, respectively

Figure 3.
Test problem for the solution of equation (4) for an inclined interface between two domains of an equal average thickness

Computational parameters

We carry out the simulations for two liquids, which are water and silicon oil, while the gas is air. Their properties are chosen at $T_w = 23°C$. The calculations are performed for two types of wall structures. The first wall (Figure 1) corresponds to the experiments reported in Alexeev *et al.* (2005) with $d = 1\,\text{mm}$, $h_w = 0.5\,\text{mm}$ and $\phi = 30°$. The second wall is given by:

$$y_w = A\left[1 - \cos\left(\frac{2\pi x}{d}\right)\right], \tag{17}$$

where $A = h_w/2$ is the wall structure amplitude. Properties of the wall material are those of copper. We also set in all our calculations $h_g = 0.4\,\text{mm}$.

We perform the calculations for a half of the groove. The computational domain is $0 \le x \le d/2$ and $0 \le y \le (h_w + \Delta h^* + h_g)$ (Figure 1). Our rectangular computational grid usually consists of 96×96 cells. To test the grid quality its density was increased, indicating that an increase in grid density practically does not affect the solution.

The calculations are started with zero initial velocities and continued up to the moment when a steady state solution is obtained.

Results and discussion

Model validation

We first consider thermocapillary convection in a rectangular cavity due to a temperature difference between the sidewalls. In the limit of thin film within a wide cavity, this problem can be solved analytically (Levich, 1962) and, therefore, can serve as a test case for our numerical model. Figure 4(a) and (b) shows the velocity and temperature distributions within the cavity for silicon oil and water, respectively. As expected, the thermocapillary force induces vortexes within the fluids in which the flow near the interface is directed toward the wall having lower temperature. Note that the isotherms within the silicon oil (Figure 4(a)) are practically vertical that corresponds to the conducting solution, while in Figure 4(b) for water, they are considerably distorted by the flow. This difference arises because water has a lower Prandtl number as compared to the silicon oil.

Figure 5 shows the pressure distribution along the gas-liquid interface the solutions shown in Figure 4 as well as the theoretical prediction (Levich, 1962). As seen, there is good agreement between the numerical solutions and the theory. Some discrepancy near the sidewalls can be attributed to the fact that the free surfaces are deformed by the flow, while the theory neglects this effect.

To verify our numerical model for the case when the thermocapillary convection is driven by a vertical temperature gradient, we first consider a rectangular cavity and estimate the critical Marangoni number M_{cr} corresponding to the onset of thermocapillary convection (Colinet *et al.*, 2001). The Marangoni number is given by:

$$M = \frac{\sigma_T \Delta T_1 \Delta h}{\rho_1 \nu_1 \alpha_1}, \tag{18}$$

where $\Delta T_1 = \Delta T Bi(1 + Bi)^{-1}$ is the temperature drop over the liquid, α the thermal diffusivity, Δh the average thickness of the liquid film and $Bi = \lambda_0 \Delta h / \lambda_1 h_g$ the Biot number. In our simulations, we found good agreement with the linear theory (Colinet *et al.*, 2001). Namely, for M less than the theoretical value of M_{cr} (Colinet *et al.*, 2001), an initial disturbance introduced into the conducting temperature distribution decays and the fluid flow stops after a transient, while for $M > M_{cr}$, steady vortexes develop.

For more thorough model validation in the case of heated grooved walls, we conducted experiments with a thin film of silicon oil (5cSt) on a wall with a structure shown in Figure 1. In the experiments, we measured temperature of the film as well as

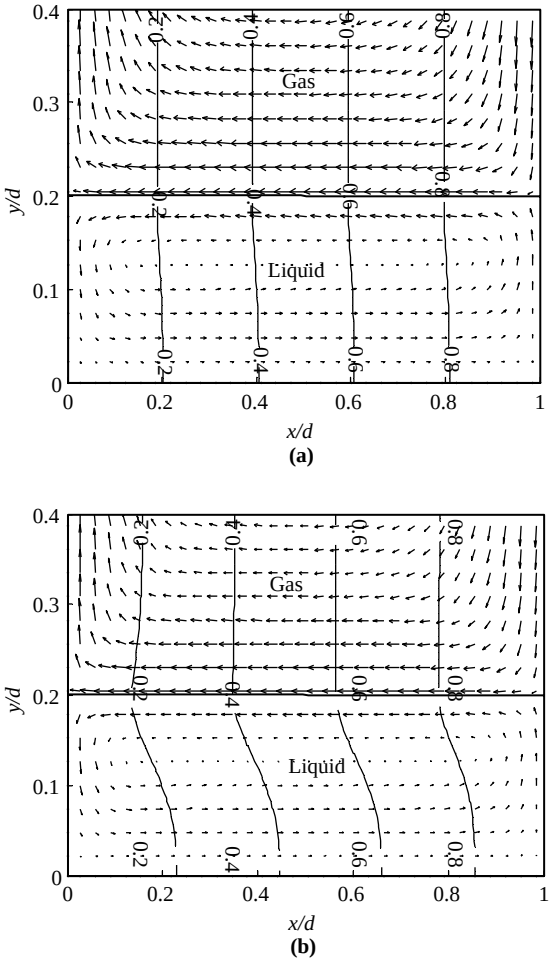

Figure 4.
Velocity and temperature distributions within a liquid film in a rectangular cavity due to a thermocapillary flow induced by a temperature difference between the sidewalls

Notes: ΔT = 1K, h = 0.1 mm, d = 0.5mm. The liquids are: (a) silicon oil; and (b) water. The arrows show the velocity field. The thin lines represent isotherms. The temperature is normalized as $(T - T_w)/\Delta T$

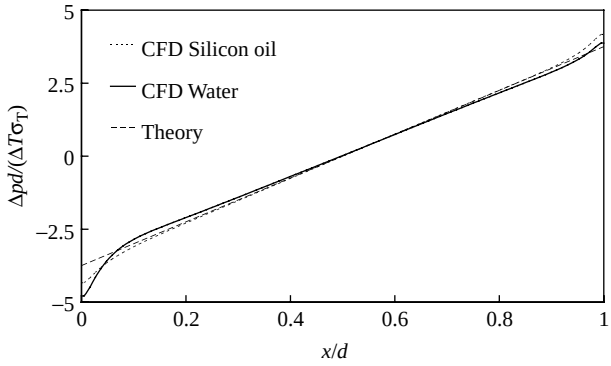

Notes: ΔT = 1K, h = 0.1 mm, d = 0.5 mm

Figure 5.
Pressure distribution along the gas-liquid interface in a rectangular cavity due to a temperature difference between the sidewalls

its maximal velocity. A detailed description of the experimental setup and the procedure can be found elsewhere (Alexeev *et al.*, 2005).

Figure 6 shows a numerically calculated flow pattern for $M \approx 1 \ll M_{cr}$. The simulation predicts the formation of a vortex, in which the liquid near the free surface moves toward the groove trough at $x = 0$. This convection is induced by the thermocapillary force due to a temperature gradient along the gas-liquid interface, which is originated from the topography of the heated wall. Moreover, in agreement with the experiments (Alexeev *et al.*, 2005), our simulations predict that the convection in films on structured walls arises for any temperature difference across the film.

In Figure 7(a), we compare the experimentally measured maximal values of the liquid velocity at the gas-liquid interface, u_{max}, with the predictions of the numerical model.

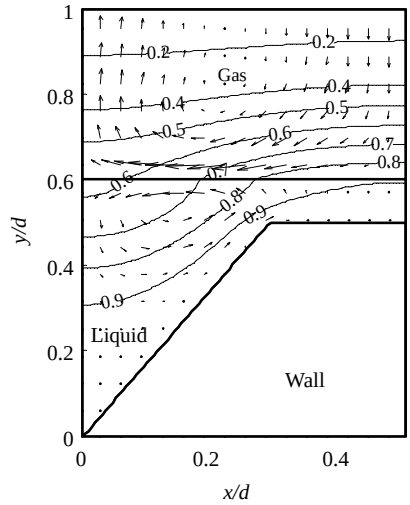

Notes: Δh^* = 0.1mm, ΔT = 1.5 K, M ≈ 1. The arrows show the velocity field. The thin lines represent isotherms. The temperature is normalized as $(T - T_w + \Delta T)/\Delta T$

Figure 6.
Velocity and temperature distributions in a silicon oil film on a structured wall (Figure 1)

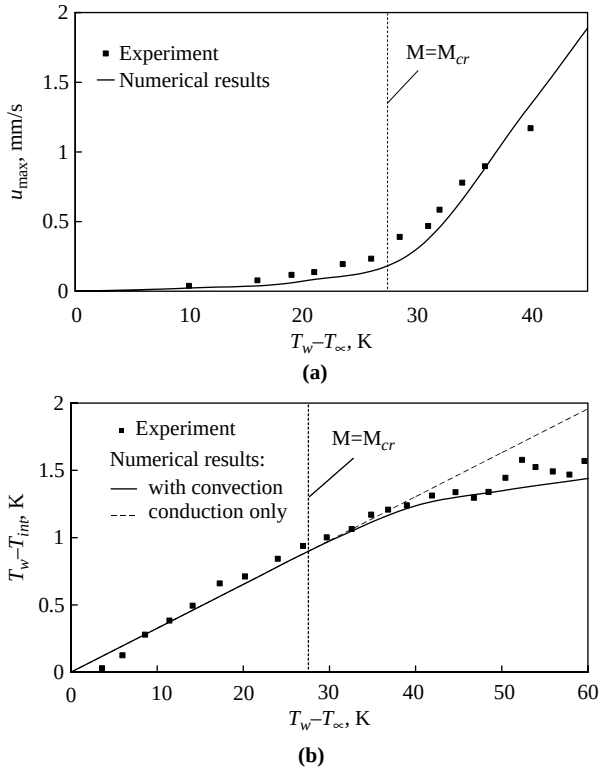

Figure 7.
(a) Maximal velocity of the liquid as a function of wall temperature;
(b) temperature drop over the liquid layer as a function of wall temperature

Notes: Silicon oil, $\Delta h^* = 0.5$ mm

One can see that there is reasonable agreement between the model and the experiments, although almost everywhere the model prediction is slightly below the experimental data. When the temperature exceeds the value corresponding to M_{cr}, the velocity increases much faster than that for the lower temperatures. It is an effect of the convective motion within the liquid layer on heat transfer. Indeed, the circulations in the layer bring hotter liquid from the hot wall to the interface, thus increasing the temperature gradient and the thermocapillary force that in turn increases the velocity.

Figure 7(b) shows the measured and calculated temperature drop across the liquid film as a function of the wall temperature. To demonstrate the effect of the convection on heat transfer, the temperature drop is also calculated when the convective terms are omitted from equation (4). In this case, the temperature drop increases linearly with T_{w}, while in the calculations with the convection terms and in the experiments, the temperature drop declines from the straight line for $M > M_{\mathrm{cr}}$. This result suggests that there is an increase in heat transfer due to the Marangoni convection within the liquid.

We conclude that the overall agreement between our calculations and the theory and experiments is rather convincing, and our numerical model may be applied to study thermocapillary flows within thin films on structured walls. In what follows, we present some numerical solutions, which are characteristic of such flows.

Flow velocities

Figure 8 shows the dependence of u_{max} on the Marangoni number. In Figure 8(a), the temperature drop is fixed at $\Delta T = 10\,\mathrm{K}$ and M changes due to Δh^*. In Figure 8(b), M increases due to the increasing temperature difference, while the other parameters are constant.

As seen in Figure 8(a), all the data collapse into a single curve. For $M > 100$, $u_{max} \sim \alpha_1 \Delta h^{-1} M^{1/2}$. Taking into account that $\Delta T = \mathrm{const}$, we obtain that M changes as Δh^2, and, therefore, $u_{max} \sim \mathrm{const}$. It means that for larger M, u_{max} practically does not depend on the thickness of the liquid layer.

The temperature difference ΔT, however, does modify the velocity as shown in Figure 8(b). Note that u_{max} grows exponentially with increasing M. It is interesting that for different Δh^*, u_{max} follows a common curve. Our calculations show that for $\Delta h^* = \mathrm{const}$, $u \sim \Delta T^{2/3}$.

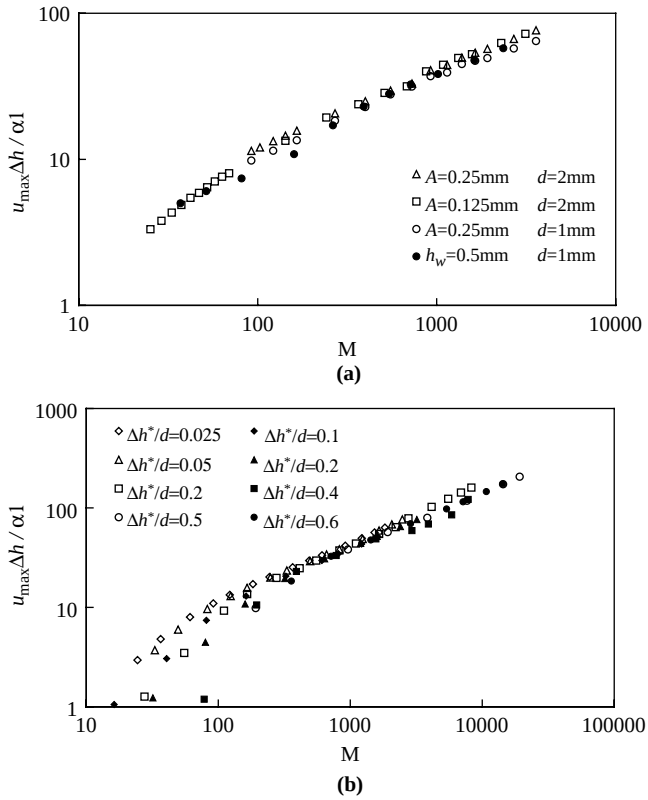

Notes: The liquid is water. The empty markers denote calculations for a sinusoidal wall profile, while the full markers stand for calculations with a wall shown in Figure 1: (a) $\Delta T = 10\mathrm{K}$; (b) $A = 0.25\,\mathrm{mm}$, $d = 2\,\mathrm{mm}$

Figure 8.
Maximal velocity of liquid vs the Marangoni number

Temperature transient

The simulations show that when the wall temperature increases suddenly, the liquid film may be ruptured as shown in Figure 9. In this simulation, uniform initial temperature equal to $T_w - \Delta T$ is imposed. At $t = 0$, T_w is applied at $y = 0$. The rupture is caused by a large temperature gradient along the free surface, which is induced when the thermal boundary layer initially formed along the liquid-wall interface reaches the gas-liquid interface near the groove crest.

We note that for the parameters in Figure 9, a steady state solution may be obtained either by a steady increase in the wall temperature or when the temperature change takes place at gas above the film. In the latter case, a thermal boundary layer is formed first at the gas-liquid interface. The temperature propagates perpendicular to the free surface, preventing the appearance of strong temperature gradients causing the rapture.

Heat transfer

Figure 10 shows the Nusselt number as a function of Δh^* for water and silicon oil. In these calculations, we consider a wall having a structure shown in Figure 1, which is either heated or cooled.

When $\Delta T = -10\,\mathrm{K}$, i.e. the wall is cooled, *Nu* exceeds unity by few percents for small Δh^* only, while for larger Δh^*, *Nu* is practically equal to unity. Thus, the effect of convection on heat transport from a cooled structured wall is relatively weak and prevails for small Δh^* only.

For a heated wall, however, our simulations predict that heat transfer can be significantly enhanced by the Marangoni convection within the film. In this case, *Nu*

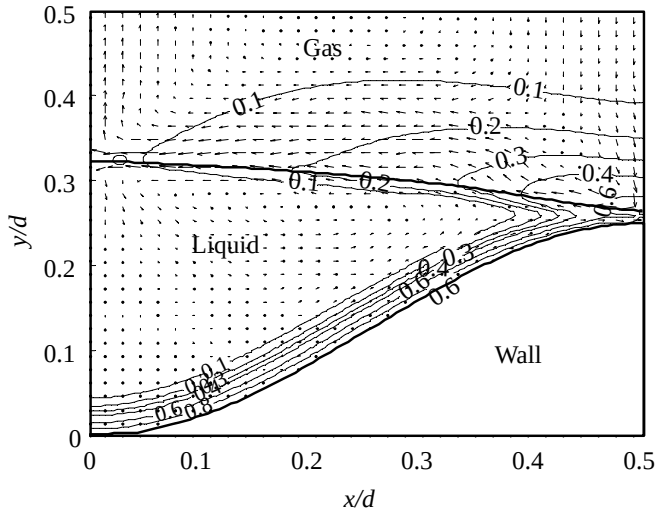

Figure 9.
Velocity and temperature distribution in a liquid film just before rupture due to an abrupt increase in wall temperature

Notes: The temperature drop ΔT = 87K (M = 1,435) corresponds to the minimal temperature at which a water film with Δh^* = 0.1 mm is ruptured on a sinusoidal wall with A = 0.25 mm, d = 2 mm. The arrows show the velocity field.The thin lines represent isotherms. The temperature is normalized as $(T - T_w + \Delta T)/\Delta T$

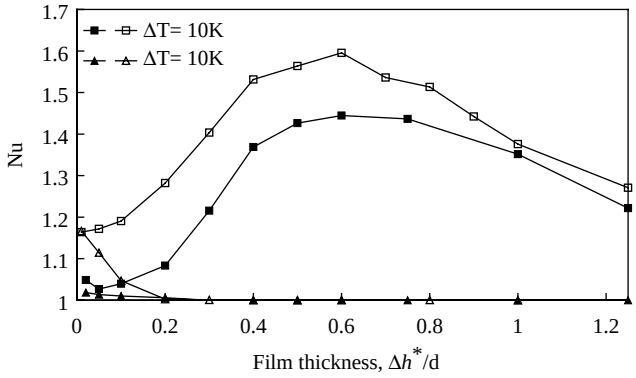

Notes: The liquid is water. The empty markers denote calculations for a sinusoidal wall with $A = 0.25$ mm, $d = 1$ mm. The full markers stand for calculations with a wall shown in Figure 1

Figure 10.
Numerically calculated Nusselt number as a function of film thickness

has maximum, which occurs for about the same optimal film thickness Δh^*_{opt} for both liquids. Thus, Δh^*_{opt} corresponds to a layer thickness, for which the effect of convection on heat transfer is most pronounced. Our simulations show that if $\Delta h^* > \Delta h^*_{opt}$, a stagnant layer of liquid is formed under the vortexes attached to the gas-liquid interface. This stagnant layer reduces the convective heat transfer from the wall, resulting in a decrease in *Nu*.

We also note in Figure 10 that the sinusoidal wall provides better convective heat transport compared to the experimental wall. Thus, an appropriate choice of the structure can enhance heat transfer in thin liquid films on structured walls.

Summary

We study thermocapillarity-induced flow of thin liquid films covering heated horizontal walls with 2D topography. To this end, we develop a numerical model based on the integration of the Navier-Stokes and energy equations by a finite difference algorithm. The mobile gas-liquid interface is tracked with the VOF technique. The numerical model is verified by comparison with a theory and experiments showing good agreement.

We demonstrate that convective motion within a film on a structured wall exists at any nonzero Marangoni number. The motion is caused by surface tension gradients induced by temperature differences at the gas-liquid interface due to the spatial structure of the heated wall. Our simulations predict that the maximal flow velocity, which occurs at the gas-liquid interface, is practically independent from the thickness of the liquid layer, and increases according to a power-law with increasing ΔT.

It is found that an abrupt change in wall temperature causes rupture of the liquid film near the structure crest. The rupture may occur at the same value of ΔT, for which a steady state solution exists and can be obtained either by a gradual increase in wall temperature or cooling gas above the liquid.

We show that the thermocapillary convection notably enhances heat transfer in liquid films on heated structured walls. An optimal film thickness exists for which *Nu* attains the maximal value for a specific temperature drop.

References

Alexeev, A., Gambaryan-Roisman, T. and Stephan, P. (2005), "Marangoni convection and heat transfer in thin liquid films on heated walls with topography: experiments and numerical study", *Physics of Fluids*, Vol. 17, pp. 062106-13.

Colinet, P., Legros, J.C. and Velarde, M.G. (2001), *Nonlinear Dynamics of Surface-Tension-Driven Instabilities*, Wiley, New York, NY.

Ferziger, J.H. and Peric, M. (2002), *Computational Methods for Fluid Dynamics*, Springer, New York, NY.

Kothe, D.B. and Mjolsness, R.C. (1992), "RIPPLE: a new model for incompressible flows with free surfaces", *AIAA Journal*, Vol. 11, pp. 2694-700.

Levich, V.G. (1962), *Physicochemical Hydrodynamics*, Prentice-Hall Inc., Englewood Cliffs, NJ.

Mehdi-Nejad, V., Mostaghimi, J. and Chandra, S. (2005), "Modeling interfacial heat transfer from single or multiple deforming droplets", *International Journal of Computational Fluid Dynamics*, Vol. 19, pp. 105-13.

Pearson, J.R.A. (1958), "On convection cells induced by surface tension", *Journal of Fluid Mechanics*, Vol. 4, pp. 489-500.

Sasmal, G.P. and Hochstein, J.I. (1994), "Marangoni convection with a curved and deforming free surface in a cavity", *ASME Journal of Fluids Engineering*, Vol. 116, pp. 577-82.

Scardovelli, R. and Zaleski, S. (1999), "Direct numerical simulation of free-surface and interfacial flow", *Annual Review of Fluid Mechanics*, Vol. 31, pp. 567-603.

Shu, C.-W. and Osher, S. (1988), "Efficient implementation of essentially non-oscillatory shock-capturing schemes", *Journal of Computational Physics*, Vol. 77, pp. 439-71.

Sussman, M. (2003), "A second order coupled level set and volume-of-fluid method for computing growth and collapse of vapor bubbles", *Journal of Computational Physics*, Vol. 187, pp. 110-36.

Wang, G. (2002), "Finite element simulations of free surface flows with surface tension in complex geometries", *ASME Journal of Fluids Engineering*, Vol. 124, pp. 584-94.

Wesseling, P. (1991), *An Introduction to Multigrid Methods*, Wiley, New York, NY.

Corresponding author
P. Stephan can be contacted at: pstephan@ttd.tu-darmstadt.de